Polarization resolved magneto-Raman scattering of graphene-like domains on natural graphite

M. Kühne,[1] C. Faugeras,[1, *] P. Kossacki,[1, 2] A. A. L. Nicolet,[1] M. Orlita,[1, 3] Yu. I. Latyshev,[4] and M. Potemski[1]

[1]*LNCMI-CNRS (UJF, UPS, INSA), BP 166, 38042 Grenoble Cedex 9, France*
[2]*Institute of Experimental Physics, University of Warsaw, Hoza 69, 00-681 Warsaw, Poland*
[3]*Institute of Physics, Charles University, Ke Karlovu 5, 121 16 Praha 2, Czech Republic*
[4]*Institute of Radio Engineering and Electronics, RAS, Mokhovaya 11-7, 125009, Moscow, Russia*

(Dated: February 25, 2013)

The micro-Raman scattering response of a graphene-like location on the surface of bulk natural graphite is investigated both at $T = 4.2$ K and at room temperature in magnetic fields up to 29 T. Two different polarization configurations, co-circular and crossed-circular, are employed in order to determine the Raman scattering selection rules. Several distinct series of electronic excitations are observed and we discuss their characteristic shapes and amplitudes. In particular, we report a clear splitting of the signals associated with the inter-Landau level excitations $-n \rightarrow +n$. Furthermore, we observe the pronounced interaction of the zone-center E_{2g}-phonon with three different sets of electronic excitations. Possible origins for these graphene-like inclusions on the surface of bulk graphite are discussed.

PACS numbers: 73.22.Lp, 63.20.Kd, 78.30.Na, 78.67.-n

I. INTRODUCTION

Raman scattering is a powerful technique that provides information concerning single particle and collective excitations in solids.[1] Phonon excitations in graphene based systems have been widely studied in the last years[2] providing a comprehensive understanding of the graphene phonon band structure,[3,4] of the different Raman scattering mechanisms and of the effect of the stacking on the observed spectrum in the case of multilayer graphene specimens.[5] This technique has recently been extended to address electronic excitations in carbon based systems.

Indirect signs of electronic excitations have first been observed on the evolution of the the E_{2g} phonon feature (G band feature) as a function of some specific thermodynamical parameter. The energy of the G band feature is mainly determined by the strong C-C bond and by the graphene crystal hexagonal symmetry, but also by the electron-phonon interaction, which can be tuned by changing the Fermi energy[6–10] or by modifying the electronic density of states by applying a magnetic field perpendicular to the plane of a graphene crystal. The $B = 0$ monotonic electronic excitation spectrum then transforms into excitations among discrete Landau levels (LL), with energies $E_{\pm n} = \pm v_F\sqrt{2e\hbar Bn}$ with $n = 0, 1, 2 \ldots$. This LL spectrum is determined by a single parameter, the Fermi velocity v_F. By increasing the magnetic field intensity, inter Landau level excitations can be tuned in resonance with the phonon which displays the so-called magneto-phonon effect.[11–15]

Raman scattering from electronic excitations have been directly observed in metallic single wall carbon nanotubes[16], in bulk graphite[17–19] and in graphene-like inclusions on the surface of bulk graphite.[15] Raman scattering techniques combined with high magnetic fields are now established as being an extremely well adapted tool to perform the Landau level spectroscopy, to explore the details of the electronic excitation spectrum and of the electron-phonon coupling in these systems. Such experiments are performed in the visible range of energy and benefit from the particularly efficient focusing and polarization optics that are well developed in this range of energy.

In this paper, we report on a polarization resolved magneto-Raman scattering experiment performed on specific locations on the surface of bulk graphite which show a number of characteristic attributes of graphene. This work is an extension of our previous experiments[15], addressing the details of magneto-Raman scattering properties of such graphene-like locations. We interpret our results in line with other experiments[20,21] pointing towards graphene layers decoupled from the sequence of Bernal-stacked graphene layers forming bulk graphite. Low energy magneto-optical absorption experiments performed on similar domains indicate that they are quasi neutral with a carrier density of $\sim 10^9$ cm^{-2} and they are characterized by an ultra high electronic mobility exceeding 10^7 cm^{2}V^{-1}s^{-1}.[21] We focus on the electronic Raman scattering signals and their evolution with increasing magnetic fields. Our low temperature, polarization resolved measurements bring direct information concerning (i) the symmetry properties of the observed excitations, (ii) the electron-hole asymmetry and (iii) the different manifestations of the electron-phonon interaction in this graphene-based system. Interestingly, these properties can be traced even at room temperature. Despite the fact that graphene-like inclusions on the surface of bulk graphite and graphene share many properties, our detailed study of electronic excitations and their evolution with increasing magnetic field reveals a number of striking differences indicating a non-negligible interaction with the underlying graphite substrate inducing Landau level mixing.

The paper is organized as follows: we start by introduc-

ing the relevant inelastic light scattering selection rules in sec. II. We continue with a description of our experiment in sec. III, followed by a discussion of our experimental results in secs. IV and V. A summary and conclusion is given in sec. VI.

II. THEORY

One of the main advantages of Raman scattering spectroscopy for the study of low energy excitations in solids, is that it is performed in the visible range of energy allowing for the use of focusing optics. Physical systems can hence be probed locally (on the μm scale), in contrast to conventional methods of infrared magneto-spectroscopy. It also allows us to use broad-band polarizing optical elements which are largely developed in the visible range of energy. Such polarized Raman scattering experiment bring some fundamental information about the symmetry of the probed excitations. Here, we consider the quasi back-scattering Faraday geometry (back scattering geometry with the use of a high numerical aperture lens providing many different angles for the incident and collected photons) and the magnetic field is applied perpendicular to the plane of the 2D crystal. In the case of graphene subjected to a high magnetic field, the main observable excitations are optical phonons and inter Landau level electronic excitations.

Raman scattering selection rules concerning optical phonons are today well established. The Raman G band is a first-order Raman scattering process involving a doubly degenerate E_{2g} optical phonon at the Γ point of the phonon Brillouin zone. These phonons carry an angular momentum of ± 1, are observed in the crossed circular polarization configurations $\sigma \pm / \sigma \mp$ (incident polarization/outgoing polarization) corresponding to an angular momentum transfer of ± 2, and are completely suppressed in the co-circular polarization configurations $\sigma \pm / \sigma \pm$.[15,18] As discussed in Ref. 18, 22, and 23, this phonon is seen through a *weakly allowed* Raman scattering process due to the trigonal warping that provides an additional angular momentum transfer of ± 3.

Electronic Raman scattering in graphene subjected to a quantizing magnetic field involves inter-LL excitations. Raman scattering selection rules for electronic excitations have been derived theoretically for graphene[24] and for bilayer graphene[25]. In Fig. 1, we present the graphene LL fan chart and we distinguish three types of excitations according to the change in the absolute value of the LL index $\Delta|n| = |n_f| - |n_i|$ where n_f (n_i) is the index of the final (initial) LL. We label excitations $n_i \rightarrow n_f$ as L_{n_i, n_f} and $\hbar \Delta |n|$ is the angular momentum transferred from/to the electronic system during the scattering process. $\Delta|n| = \pm 2$ excitations are expected to be active in the crossed-circular polarization configuration $\sigma \mp / \sigma \pm$, and $\Delta|n| = \pm 0$ excitations in the co-circular polarization configuration $\sigma \pm / \sigma \pm$.[24]

Similar to the case of the E_{2g} phonon, scattering from
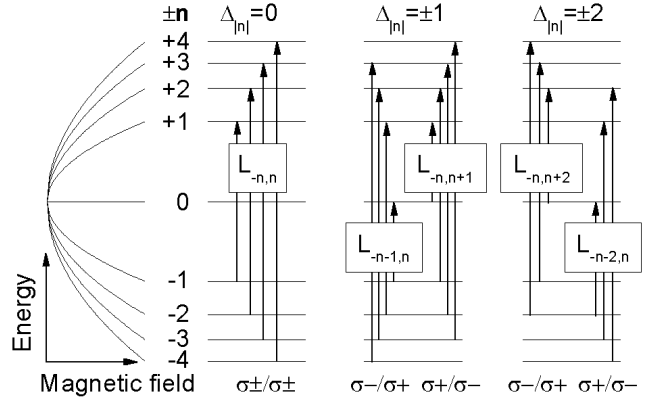

Figure 1. Schematic graphene LL spectrum with three types of electronic excitations. Selection rules for the inelastic light scattering processes are indicated.

$\Delta|n| = \pm 1$ excitations (optical-like excitations) is forbidden in the isotropic approximation but becomes allowed due to the trigonal warping that provides an additional angular momentum transfer of ± 3.[24] These excitations are hence expected to be observed in the $\sigma \pm / \sigma \mp$ polarization configuration. Kashuba and Fal'ko[24] find that the most pronounced signals from electronic Raman scattering in graphene should be due to the $\Delta|n| = 0$ excitations. Furthermore, the associated signal intensities are expected to scale $\propto B$.[24]

Interactions between electronic excitations and the E_{2g} phonon leads to a magnetic-field dependent renormalization of the phonon energy and to pronounced avoided crossings of the coupled phonon- and electronic modes.[11–15] Relevant electronic excitations for this effect are the $\Delta|n| = \pm 1$ excitations.[24] However, recent experimental results[15] suggest a violation of this selection rule in graphene-like locations found on the surface of natural graphite as $\Delta|n| = 0$ excitations were also shown to strongly interact with the phonon.

III. EXPERIMENT AND RESULTS

We have performed magneto-Raman scattering experiments in the quasi back-scattering Faraday configuration. The excitation laser beam, provided by a Ti:sapphire laser setup, was tuned to $\approx \lambda = 785$ nm. Two optical fibers with core diameters of 5 μm and 200 μm were used respectively to excite the sample and to collect the scattered light. An aspherical lens is used to focus the excitation laser to a spot of ~ 1 μm diameter. The collected signal was dispersed in a single grating spectrometer equipped with a liquid nitrogen-cooled CCD detector. The optical power on the sample was of the order of 7 mW. The sample was mounted on x-y-z piezo-stages, immersed in a low-pressure He atmosphere kept at $T = 4.2$ K (except for room temperature experiments) and placed in the center of a resistive magnet delivering

continuous magnetic fields up to 29 T. A set of optical filters was used to minimize the contribution of superfluous light (Raman signals from the fibers, stray light etc.) to the spectra. Experiments have been performed both in the co-circular polarization configurations ($\sigma\pm/\sigma\pm$) and in the crossed-circular polarization configurations ($\sigma\pm/\sigma\mp$). Both pairs of circular polarization configuration, e.g., $\sigma+/\sigma+$ and $\sigma-/\sigma-$ in the case of the co-circular configuration, were achieved by inverting the polarity of the magnetic field with respect to the light propagation direction.

The sample used in this experiment is a piece of natural graphite. Graphene-like locations are identified on the surface of bulk graphite using the method described in Ref. 15. Accordingly, we laterally map the Raman scattering response of the sample subjected to a finite magnetic field. The field strength is chosen so that the G band energy is significantly modified with respect to its $B = 0$ T energy due to the electron-phonon interaction. This method is straightforward and unambiguous especially since the amplitude of the energy renormalization of the G band in graphite is much smaller than in graphene, because of the 3D Landau bands in the underlying graphite substrate.[18]

In Fig. 2 we show several raw spectra (black lines) of the magneto-Raman scattering response of such a graphene-like location as measured in the two polarization configurations at $T = 4.2$ K. Apart from a relatively flat background, these spectra are affected by a parasitic signal extending from ~ 1200 cm^{-1} to ~ 1900 cm^{-1} possibly due to inelastic scattering or luminescence contributions from one of the optical elements or optical fibers used in the set-up. However, since this signal only shows a weak, and to a first approximation linear, dependence on the magnetic field, we can correct our spectra by subtracting, for each energy, a linear in magnetic field background (red dashed lines in Fig. 2(c)). The result of such a correction is shown as blue lines in Fig. 2). in the following, we mainly take advantage of the better contrast obtained through this correction in order to plot intensity false color maps, while we use uncorrected spectra to discuss the details of line shapes and intensities.

An overview of our experimental results is shown in Fig. 3. Figs. 3(a) and 3(b) are intensity false color maps of the background corrected spectra measured in the co-circular configuration and in the crossed-circular configuration, respectively, as a function of $\sqrt{B}$. Correspondingly, we present some individual spectra without any background subtraction in Fig. 4(a) and with background subtraction in Fig. 4(b) slightly affecting the intensities in the gray shaded region. Figs. 3 and 4 clearly demonstrate that various magnetic field-dependent signals characterized by different line shapes are observed in the Raman scattering response of our sample, and that these different signals are selected by the two distinct polarization configurations. Similar results have been obtained on 4 different pieces of natural graphite and on HOPG. We limit all discussions in this paper to the graphene-like excitations. The Raman scattering response from the underneath graphite substrate, which is also observed when placing the laser spot on a graphene-like domain and which is indicated by the diagonal arrows in Fig. 3, has been discussed in details in Ref. 18.

IV. CO-CIRCULAR CONFIGURATION

We present in Fig. 3(a) a false color map of the scattered intensity as a function of the magnetic field measured in the co-circular polarization configurations. Several series of magnetic field dependent features can be identified. Their characteristic, in a first approximation, $\sqrt{B}$ evolution indicates that they arise from electronic excitation among graphene LLs. The most pronounced features correspond to inter-LL excitations of the type $L_{-n,n}$. Their evolution with increasing magnetic fields can be described (full white lines in Fig. 3(a)) by the graphene LL spectrum given by $E_{\pm n} = \pm v_F\sqrt{2e\hbar Bn}$ with $n = 0, 1, 2\ldots$ and a Fermi velocity $v_F = (1.04 \pm 0.03)\cdot 10^6$ m$\cdot$s^{-1}. Results obtained in the $\sigma+/\sigma+$ and in the $\sigma-/\sigma-$ configurations are identical within the resolution of our experiment. Our measurement further confirms that inelastic light scattering involving this kind of electronic excitations is allowed in the co-circular configuration, as expected from the zero angular momentum transfer.

However, a detailed analysis of these Raman scattering spectra reveals that to properly describe the magnetic field evolution of the $L_{-n,n}$ series, an energy dependent v_F has to be used. This is particularly visible in the case of the $L_{-1,1}$ feature in Fig. 3(a). As shown in Fig. 6(d), the Fermi velocity v_F decreases by $\sim 5\%$ as the energy of $L_{-1,1}$ shifts from 110 meV to 280 meV. Recent magneto-transport experiments performed with suspended, high mobility graphene specimens have revealed an electron-electron interactions induced increase of the Fermi velocity, of nearly a factor 3, as a function of the Fermi energy[26], in agreement with theoretical predictions.[27,28] The graphene system studied here shows an increase of $\sim 5\%$ of the Fermi velocity that could be strongly reduced, in this frame, by the underlying graphite substrate efficiently screening Coulomb interaction. In contrast to Ref. 26, our magneto-Raman scattering experiment probes the evolution of the different electronic states versus energy at a fixed Fermi energy.

As can be seen in Fig. 4(a), the amplitudes of the different $L_{-n,n}$ excitations clearly depend on both the magnetic field and on the LL index n. At a given value of the magnetic field, the frequency-integrated intensity $I(L_{-1,1})$ is bigger than $I(L_{-2,2})$ which is in turn bigger than $I(L_{-3,3})$. The integrated intensities of these three excitations, extracted from the measured spectra and corrected for the wavelength dependence of the quantum efficiency of our CCD camera, are shown in Fig. 5. As can be seen in this Figure, the intensity of each $L_{-n,n}$ transition scales $\propto B$ in agreement with theory[24]. In ad-
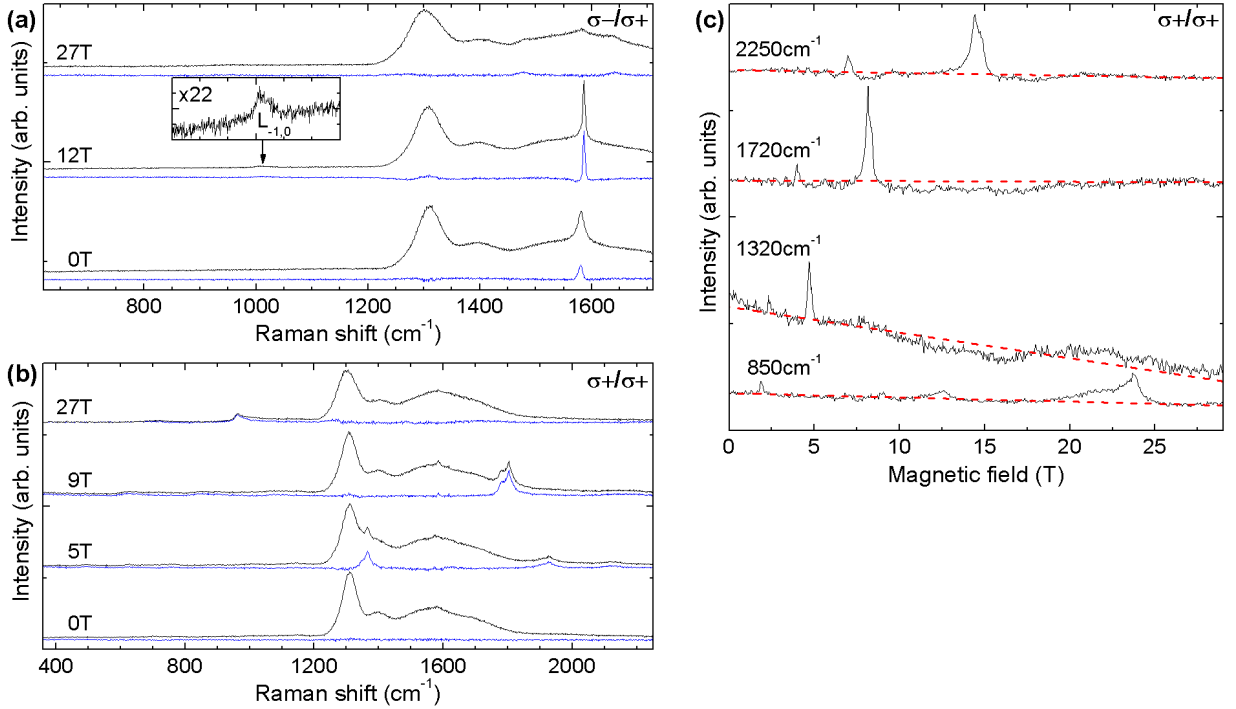
Figure 2. (Color online) Raw data spectra (black lines) measured at different values of the magnetic field in the (a) crossed-circular configuration and (b) co-circular configuration. Corrected spectra (blue lines in (a) and (b)) are obtained by subtracting a linear background (red dashed lines in (c)) from the data at each energy value.

dition, we find that $I(L_{-n,n})$ scales $\propto 1/n$. This latter fact is emphasized in Fig. 5 by multiplying all $I(L_{-n,n})$ by n.

Furthermore, the observed $L_{-n,n}$ excitations show strongly asymmetric line shapes, see Fig. 4(a). As shown in Fig. 6(a), it appears clearly that, at high magnetic fields, both $L_{-1,1}$ and $L_{-2,2}$ signals are composed of two components with one of lower amplitude at the low-energy side. This characteristic is the same in both $\sigma+/\sigma+$ and $\sigma-/\sigma-$ configuration. As demonstrated in Fig. 6(a), we quantify this phenomenon by fitting each of these $L_{-n,n}$ excitations with the sum of two Lorentzian functions. The splitting energy ΔE between the centers of the two individual Lorentzians, can then be extracted as is shown in Figs. 6(b) and 6(c) for $L_{-1,1}$ and $L_{-2,2}$, respectively. The splits are extracted from three different sets of data acquired during three consecutive measurements (two performed in $\sigma+/\sigma+$ configuration and one in $\sigma-/\sigma-$ configuration) on the same spot on the sample, to ensure reproducibility of the effect.

As can be seen in Fig. 6, the magnitude of the extracted splits increases with increasing magnetic fields. Moreover, at a given value of B, ΔE is bigger for $L_{-2,2}$ than for $L_{-1,1}$. ΔE shows a $\sqrt{B}$-dependence, indicated by the black dashed lines in Figs. 6(b) and (c). Such a magnetic field-dependence could in general be consistent with the existence of two cones with different Fermi velocities v_F1 and v_F2. In such a case, the splitting of $L_{-n,n}$ would be $\Delta E = \Delta v_F \cdot 2\sqrt{2e\hbar Bn}$, where

$\Delta v_F = |v_F1 - v_F2| \approx 0.06 \cdot 10^6$ m/s. The magnitude of ΔE would consequently depend on the LL index n, which we have taken into account for drawing the black dashed lines in Figs. 6(b) and (c). Although the physical reason for the appearance of the observed ΔE is not fully understood, we believe that it may be induced by a residual interaction with the underlying graphite substrate. The recent report of an equally unusual LL splitting induced by the twist in a graphene bilayer maybe points in the same direction.[29]

We now turn to the observation of a set of $\sqrt{B}$-dependent features that we assigned in Fig. 3(a) to $L_{-n,n+1}^{-(n+1),n}$ excitations (a regrouped form accounting for $L_{-n,n+1}$ and $L_{-(n+1),n}$). As was discussed in Sec. II, inelastic light scattering involving this type of excitations is not theoretically expected in this polarization configuration.[24] Nevertheless, we find a good agreement with our data when calculating their energies (dotted black lines) again using $v_F = (1.04 \pm 0.03) \cdot 10^6$ m/s. These features are pronounced even far away in energy from the Raman G band only for $n \geq 1$ which appear in our spectra at low values of the magnetic field, $B \leq 10$ T. The $L_{0,1}^{-1,0}$ excitation is much weaker and the associated signal can hardly be identified in the spectra (a fact especially clear for $B \geq 10$ T). Fig. 5 shows the integrated intensities of the $L_{-1,2}^{-2,1}$ and $L_{-2,3}^{-3,2}$ excitations. In comparison to the $L_{-n,n}$ series, the observed behavior for the $L_{-n,n+1}^{-(n+1),n}$ series is much less pronounced. The depen-
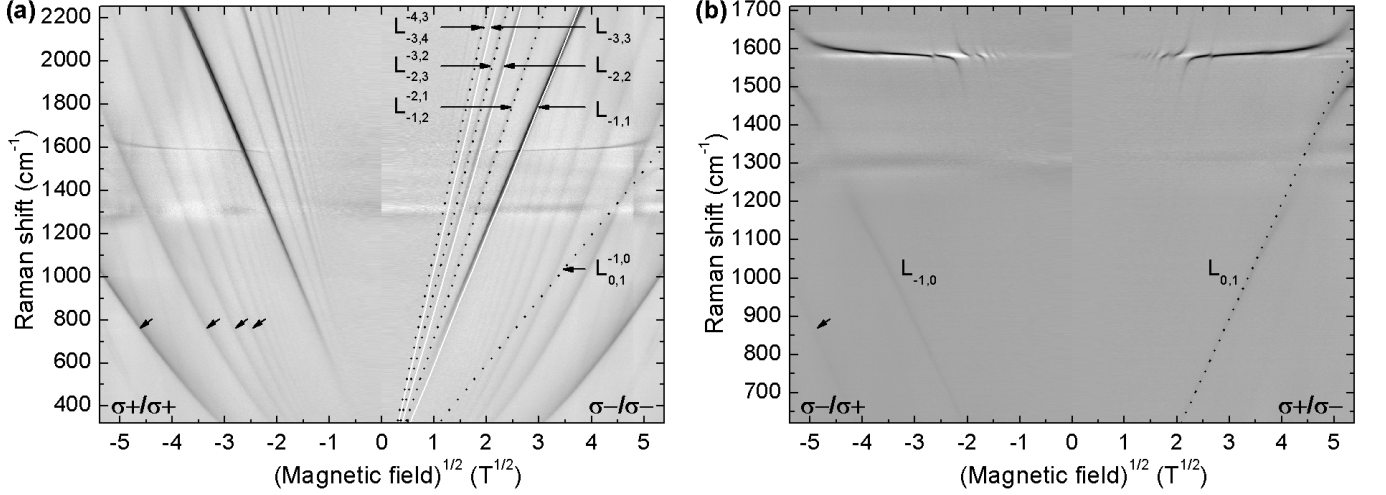
Figure 3. Magneto-Raman scattering response of graphene on natural graphite measured in (a) co-circular configuration and (b) crossed-circular configuration: Intensity false color plots of the background-corrected spectra. Black (white) corresponds to high (low) intensity.
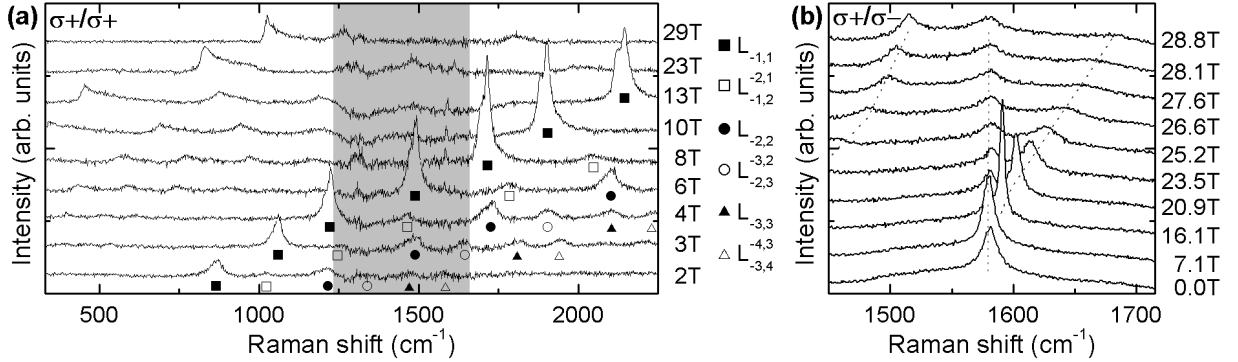

Figure 4. Magneto-Raman scattering response of graphene on natural graphite measured in (a) co-circular configuration and (b) crossed-circular configuration. The spectra in (a) are background-corrected; symbols identify signals that are due to electronic excitations in graphene. Intensities in the gray shaded region are slightly affected by the background correction described in the text. Dotted lines indicate three Raman G band components in (b).

dence of their oscillator strengths on B is certainly weak and a decrease with decreasing n could be suggested.

A remarkable aspect of the $L_{-n,n+1}^{-n-1,n}$ excitations observed in the co-circular polarization configuration is that they do not interact with the E_{2g}-phonon. This is clearly seen in Fig. 7 as the magnetic field dependence of the Raman signals associated with $L_{-n,n+1}^{-n-1,n}$ form straight lines instead of the expected avoided crossings with the phonon (compare with the weak signal from the Raman G band, visible due to a polarization leak). We therefore believe that these particular electronic excitations observed here do not have the same symmetry as the phonon, but correspond rather to the complementary set of usually infrared-active modes that are characterized by the irreducible representation (IR) E_{1u} of D_{6h}. The origin of asymmetric transitions (optical-like) which are Raman active and seen in the co-circular polarization configuration is not clear. We may only speculate that their appearance is due to Landau level mixing (transitions in-

volving higher LL indexes are more pronounced) and/or their observation is allowed for the particular graphene system studied here due to some residual interaction of the graphene flakes with the graphite substrate. Optionally, we note that those transitions are expected to be forbidden in Raman scattering processes in case of an ideal, back scattering Faraday geometry but they are perhaps active in the present measurement[30] due to an imperfection of our experimental configuration (large apertures of the excitation and of the collected light).

Finally, we measured the room temperature magneto-Raman scattering response of a similar graphene location on the surface of bulk natural graphite. In Fig. 8 we show the obtained spectra after subtraction of the zero-field scattering response in the form of an intensity false color plot. Surprisingly, although the magnetic field resolution is worse than in our low-temperature experiment, one can clearly see that the same physics is observed. Notably, Raman scattering from electronic excitations in
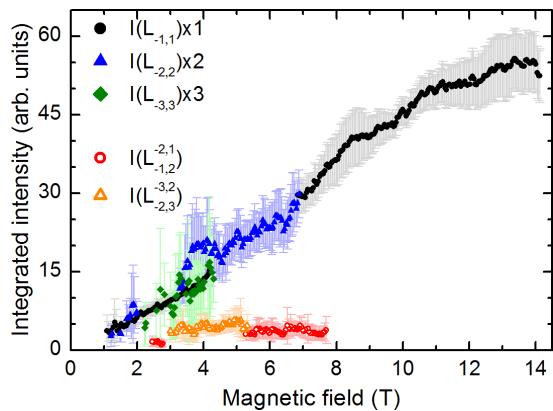
Figure 5. (Color online) Integrated intensities of the signals identified in Fig. 3(b) extracted from the data acquired in $\sigma-/\sigma-$ configuration.

graphene, discussed above, is still clearly measured up to room temperature. The intensities of the different excitations also show a behavior comparable to the one observed at $T = 4.2$ K.

V. CROSSED-CIRCULAR CONFIGURATION

Figs. 3(b) and 4(b) show the Raman scattering response of the graphene-like location measured in the crossed-circular configuration. In contrast to the co-circular configuration, the G band feature is observed[18]. When applying a magnetic field, the magneto-phonon effect[11,12] appears as an avoided crossing behavior each time the energy of specific inter-LL excitations is tuned in resonance with the phonon. As discussed further below (see Fig. 10), the most pronounced of these avoided crossings are caused by electronic excitations of the $L_{-n,n+1}^{-(n+1),n}$ series. The raw spectra in Fig. 4(b) illustrate well the magnitude of this effect for the $L_{0,1}$ excitation. These spectra, however, are resolution limited in energy. The acquisition of some high-resolution spectra showed that the full width at half maximum of the G band ($FWHM_G$) was in general much smaller than the one suggested in Fig. 4(b), as low as e.g. $FWHM_G \approx 2.5$ cm^{-1} measured at $B = 11$ T.

It should be noted, that $L_{0,1}^{-1,0}$ is in fact the only electronic excitation from which we observe inelastic light scattering, in this polarization configuration, also far away in energy from the Raman G band (see Fig. 3(b) and the inset in Fig. 2(a)). Other electronic excitations of the $L_{-n,n+2}^{-(n+2),n}$ series, expected to be active in this polarization configuration,[24] are probably too weak to be detected in our experimental setup. As shown in Fig. 3(b), apart from the $L_{0,1}^{-1,0}$ excitations, we only observe traces of Raman scattering from other electronic excitations of the $L_{-n,n+1}^{-(n+1),n}$ series close to the phonon energy with which they hybridize.

Strikingly, the magnetic field dependence of the Raman G band is not symmetric with respect to inversion of the polarization configuration. The differences in the energy of the signal between $\sigma+/\sigma-$ and $\sigma-/\sigma+$ appear especially at higher magnetic field strengths, see Fig. 3(b). To emphasize this fact, we fitted the Raman G band components with a single Lorentzian in order to extract their energy positions as shown in Fig. 9(b). The result is plotted for both $\sigma+/\sigma-$ and $\sigma-/\sigma+$ in Fig. 9(a), clearly showing the mentioned differences which reflect, as we argue, an asymmetry between electron and hole states. Finite doping could also induce differences between $\sigma+/\sigma-$ and $\sigma-/\sigma+$, however, not changing the value of the Fermi velocity by rather the magnitude of the observed anticrossings[12]. This asymmetry is caused by the trigonal warping, which in graphene is described by a second-order term in the expansion of the graphene LL energies, determined by the next-nearest-neighbor hopping integral γ_0'. In this respect, graphene differs from graphite, where the interlayer hopping parameter γ_3 is responsible for the trigonal warping. Including this term, the energies of the LLs in graphene are given by $E_{\pm n} = \pm v_F \sqrt{2e\hbar B n} + 9eB/(2\hbar)v_F\gamma_0'a_0^2 n$ where $a_0 = 1.42$ Å is the C-C distance.[31] Consequently, the energies of electronic excitations such as $L_{0,1}$ and $L_{-1,0}$ are no longer degenerated in the presence of this electron-hole asymmetry. this can be seen in Fig. 9(a) where we compare the magnetic field dependence of the energy of the degenerate $L_{0,1}^{-1,0}$ excitation (full black line) with the corrected energies of $L_{0,1}$ and $L_{-1,0}$ (dashed black lines) calculated with the parameters given in the figure. As we show below, the electron-hole asymmetry in this graphene-like system can be directly determined from the given data.

It should be noted that the oscillations of the Raman G band are in fact not as simple as theoretically expected. In Refs. 11 and 12, only electronic excitations of the type $L_{-n,n+1}^{-(n+1),n}$ are considered to hybridize with the phonon, in agreement with what is observed in multi-layer epitaxial graphene on SiC(000$\bar{1}$).[13] However, in addition to the previously measured avoided crossings caused by excitations of the $L_{-n,n+1}^{-n-1,n}$ series[14,15] and of the $L_{-n,n}$ series[15] at similar locations on bulk graphite, we find clear evidence for a further interaction due to the $L_{0,2}^{-2,0}$ excitation. This new effect is illustrated in the inset of Fig. 9(a). Similar to the mechanism invoked for the observability of electronic Raman scattering from $L_{-n,n+1}^{-n-1,n}$ excitations in the co-circular configuration, here the additional and unexpected interaction is possibly caused by the mixing of LL wave functions. In the absence of a complete theoretical model, we describe the coupling between the phonon and $L_{-n,n+1}^{-n-1,n}$ excitations in terms of the dimensionless coupling constant λ.[11,13] For all the other electronic excitations of energies $\Delta_{-n,m}$, we use magnetic field-independent effective coupling parameters $g_{-n,m}$. Thus, we can calculate the energy ϵ of the electron-phonon coupled modes by solving[11,12]
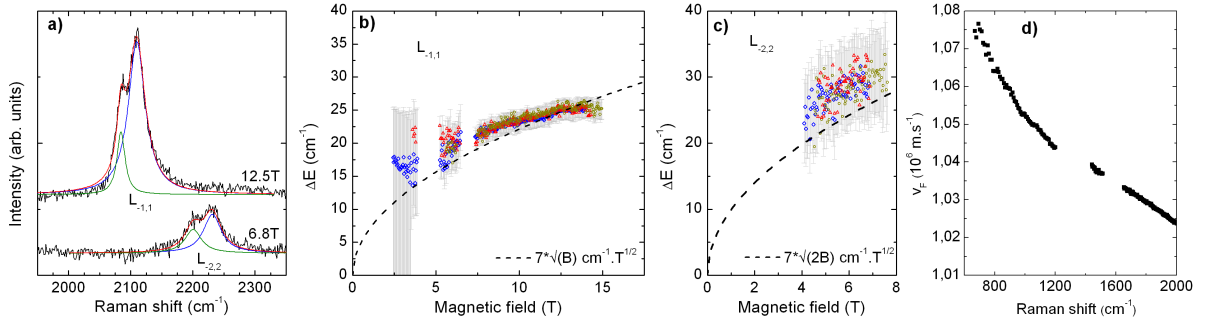
Figure 6. (Color online) (a) Measured Raman scattering response at two values of B. The signals associated with the excitations $L_{-1,1}$ and $L_{-2,2}$ are fitted with two Lorentzian functions. The split between the centers of these two Lorentzians ΔE is shown in (b) and (c) as extracted from three data sets acquired by measuring the same sample. d) Fermi velocity for the main component of the $L_{-1,1}$ as a function of the energy of the excitation.
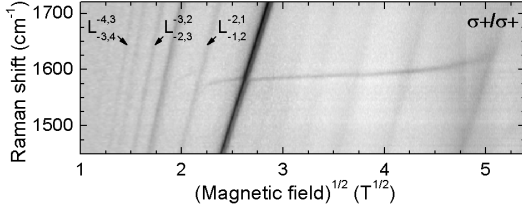

Figure 7. Raman scattering response as a function of the magnetic field: intensity false color plot as in Fig. 3(a).

$$
\epsilon^2 - \epsilon_0^2 - 4\epsilon_0 \sum_{n=0}^{n_c} \frac{\lambda}{2} E_1^2 \left(\frac{\Delta_{-n,n+1}}{\epsilon^2 - \Delta_{-n,n+1}^2} + \frac{1}{\Delta_{-n,n+1}} \right)
$$
$$
- 4\epsilon_0 \sum_{(-n,m)} g_{-n,m}^2 \left(\frac{\Delta_{-n,m}}{\epsilon^2 - \Delta_{-n,m}^2} + \frac{1}{\Delta_{-n,m}} \right) = 0,
$$
(1)

where ϵ_0 is the energy of the phonon at $B = 0$ T and where the second sum is over $L_{-1,1}$, $L_{-2,2}$, $L_{-3,3}$, $L_{0,2}$ and $L_{-2,0}$. Taking into account the electron-hole asymmetry, only one of the last two excitation is considered respectively in either $\sigma+/\sigma-$ configuration or $\sigma-/\sigma+$ configuration. The same holds for the $L_{-n,n+1}^{-n-1,n}$ excitations.

The best fit to our data, shown in Fig. 10, is obtained for the parameters given therein. $\lambda = 4.4 \cdot 10^{-3}$ is found to be in good agreement with previous experiments on such kind of graphene samples[14,15] as well as on epitaxial graphene on $SiC(000\bar{1})$[13]. The effective coupling strengths $g_{-n,n}$ are found to decrease with decreasing n as the magneto-phonon resonances take place at higher values of the magnetic field. This already observed behavior[15] is consistent with a mixing of LLs that decreases with increasing magnetic fields. The parameter $g_{0,2}^{-2,0}$ is found to be of the same order as the $g_{-n,n}$. Here, we introduced a non-zero broadening in the calculation to smear out the avoided crossing caused by $L_{0,2}^{-2,0}$, since it

is not very pronounced. In what concerns the electron-hole asymmetry, we obtain $\gamma_0' = 0.4$ eV, in agreement with tight-binding calculations.[32]

Finally, we have performed similar magneto-Raman scattering experiments at room temperature. The measured spectra, from which the scattering response at $B = 0$ T has been subtracted, are shown in the form of an intensity false color map in Fig. 11. Electronic Raman scattering far away from the Raman G band is not clearly observed, which is why the spectral range in Fig. 11 was limited to show the Raman G band, only. We qualitatively observe again the same behavior as at $T = 4.2$ K. As it was already reported in the case of K-point carriers in bulk graphite[18], avoided crossings caused by the interaction of the zone-center E_{2g}-phonon with electronic excitations $L_{0,1}$ and $L_{-1,2}$ are clearly observed at room temperature, while a trace of the interaction with $L_{-1,1}$ is also seen.

VI. SUMMARY AND CONCLUSION

We have discussed the magneto-Raman scattering response of graphene on natural graphite measured in two different polarization configurations: co-circular and crossed-circular. Scattering signals from phonon- as well as from electronic excitations of different types are identified in the data obtained in the two configurations, allowing to verify the different selection rules of the related scattering processes. The most pronounced electronic Raman scattering signals are measured in the co-circular configurations and they are due to electronic excitations among LLs of graphene which are symmetric with respect to the LL index, i.e. $L_{-n,n}$. The integrated intensities of these signals are found to scale $\propto B/n$. Furthermore, the strongest two of these excitations show a clearly asymmetric line shape that depends on the applied magnetic field strength B. In the crossed-circular configuration, the dominant feature measured is the G band which shows a series of avoided crossings as a function of B. The
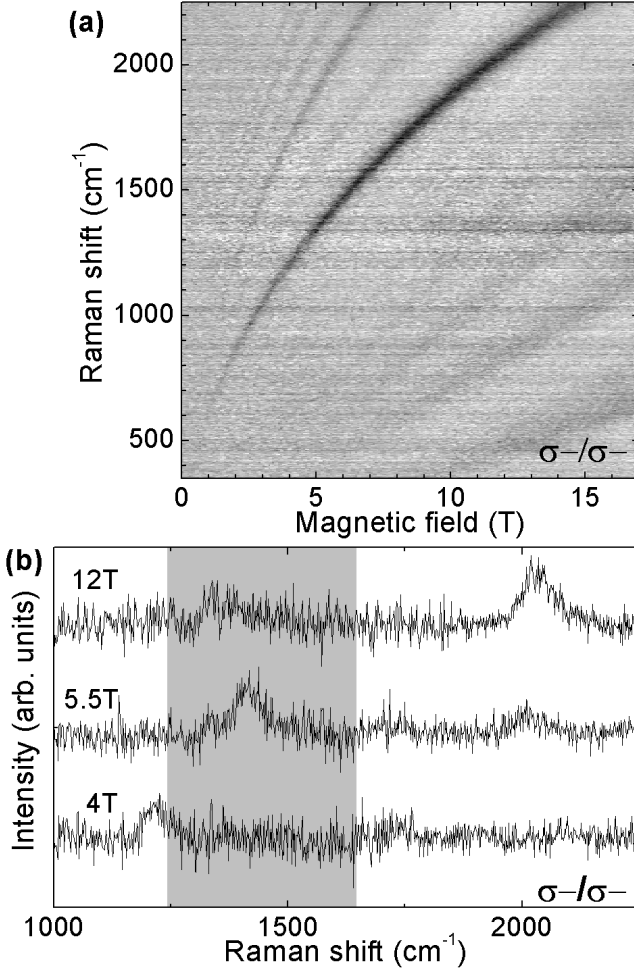
Figure 8. Room temperature magneto-Raman scattering response in co-circular configuration: (a) intensity false color plot where black (white) corresponds to high (low) intensity and (b) individual, background-corrected spectra.

$L_{0,1}^{-1,0}$ is the only electronic excitation observed far away from the phonon feature in this configuration. The E_{2g}-phonon in this graphene system interacts with the different electronic excitations $L_{-n,n}$, $L_{-n,n+1}^{-n-1,n}$ as well as with $L_{0,2}^{-2,0}$. We quantify the interaction strengths associated with the different excitations and additionally extract the next-nearest-neighbor hopping energy γ_0' that describes the electron-hole asymmetry in graphene. The unexpected observation, namely the G band avoided crossings caused by other than $L_{-n,n+1}^{-n-1,n}$ excitations as well as the Raman scattering signals in the co-circular configuration we assigned to usually infrared-active electronic modes, are both possibly related to a residual interaction between the graphene flake and the graphite substrate on which it lies, and to the quasi backscattering configuration used in this experiment. While the discussions in this report were mainly focused on results obtained from measurements performed at 4.2 K, we show that most of these properties persist up to room temperature. This
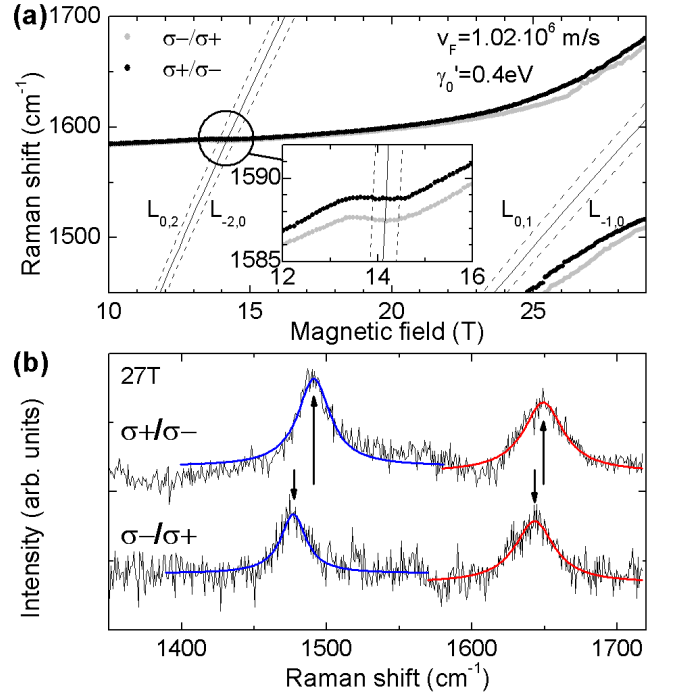

Figure 9. (a) Energy positions of the Raman G band in $\sigma+/\sigma-$ and $\sigma-/\sigma+$ extracted from the background-corrected spectra by doing single-Lorentzian fits as demonstrated in (b). Energies of some electronic excitations (dashed lines) corrected by a finite γ_0' as compared to the case of $\gamma_0' = 0$ (full lines, degenerate excitations).

holds especially as we readily observe Raman scattering from electronic excitations as well as the characteristic magnetic-field induced oscillations in the G band feature, both at room temperature.

Our magneto-Raman scattering experiment presented here cannot unambiguously determine the nature of these graphene-like locations. The response from bulk graphite is also observed on such locations giving an indication on the relatively small thickness of the region of interest. Recent tight binding calculations of the band structure of AA stacked graphite[33] show that this material host Dirac fermions along the **HKH** corner of its Brillouin with Fermi velocities differing by 3%, in line with the splitting of the $L_{-n,n}$ excitations observed in this work. Nevertheless, the value of the Fermi energy at the **H** and **K** points are not compatible with the observation of any inter Landau level excitations below ~ 800 meV. The most probable scenario is that the first graphene layer does not follow the Bernal stacking sequence and is twisted with respect to the underlying layer. The electronic properties of such twisted graphene bilayers have recently been the subject of intense theoretical research[34], indicating not only a renormalization of the Fermi velocity[35] but the existence of two distinct cones with different Fermi velocities.

To conclude, by using polarization-resolved magneto-Raman scattering techniques, we have experimentally
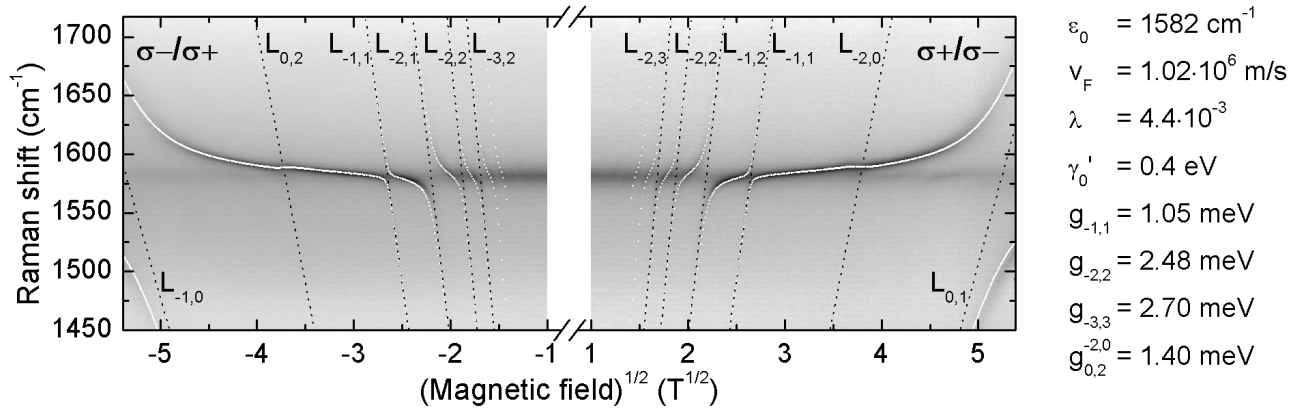
Figure 10. Magneto-Raman scattering response: Intensity false color plot where black (white) corresponds to high (low) intensity. Black dotted lines are the energies of the inter-LL excitations that interact with the zone-center E_{2g}-phonon. White dots are solutions to Eq. (1) calculated with the parameters given on the right.
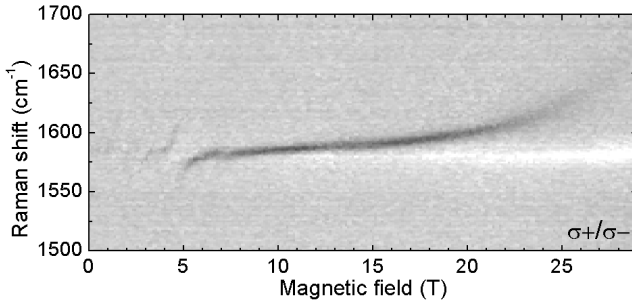

Figure 11. Room temperature magneto-Raman scattering response: Intensity false color plot where black (white) corresponds to high (low) intensity measured in the crossed-circular configuration.

phonon- and electronic excitations. Interactions between both types of excitations have been quantified as was the electron-hole asymmetry in our sample, which could be directly measured and expressed in terms of the next-nearest-neighbor hopping energy γ_0'. We furthermore demonstrated that LL spectroscopy using magneto-Raman scattering in graphene can be performed at room-temperature.

VII. ACKNOWLEDGEMENTS

determined Raman scattering selection rules for different inelastic light scattering processes in graphene-like domains at the surface of bulk graphite involving both

* clement.faugeras@lncmi.cnrs.fr

[1] M. Cardona, ed., *Light Scattering in Solids 1*, 2nd ed., Topics in Applied Physics, Vol. 8 (Springer-Verlag, 1983).

[2] A. Jorio, M. Dresselhaus, R. Saito, and G. F. Dresselhaus, *Raman Spectroscopy in Graphene Related Systems* (Wiley-VCH, 2011).

[3] A. C. Ferrari, J. C. Meyer, V. Scardaci, C. Casiraghi, M. Lazzeri, F. Mauri, S. Piscanec, D. Jiang, K. S. Novoselov, S. Roth, and A. K. Geim, Phys. Rev. Lett. **97**, 187401 (2006).

[4] D. L. Mafra, G. Samsonidze, L. M. Malard, D. C. Elias, J. C. Brant, F. Plentz, E. S. Alves, and M. A. Pimenta, Phys. Rev. B **76**, 233407 (2007).

[5] C. Faugeras, A. Nerrière, M. Potemski, A. Mahmood, E. Dujardin, C. Berger, and W. A. de Heer, Appl. Phys.

Lett. **92** (2008).

[6] T. Ando, J. Phys. Soc. Jpn. **75**, 124701 (2006).

[7] M. Lazzeri and F. Mauri, Phys. Rev. Lett. **97**, 266407 (2006).

[8] S. Pisana, M. Lazzeri, C. Casiraghi, K. Novoselov, A. Geim, A. Ferrari, and F. Mauri, Nat. Mater. **6**, 198 (2007).

[9] J. Yan, Y. Zhang, P. Kim, and A. Pinczuk, Phys. Rev. Lett. **98**, 166802 (2007).

[10] A. Das, S. Pisana, B. Chakraborty, S. Piscanec, S. K. Saha, U. V. Waghmare, K. S. Novoselov, H. R. Krishnamurthy, A. K. Geim, A. C. Ferrari, and A. K. Sood, Nat. Nano. **3**, 210 (2008).

[11] T. Ando, J. Phys. Soc. Jpn. **76**, 024712 (2007).

[12] M. O. Goerbig, J.-N. Fuchs, K. Kechedzhi, and V. I. Fal'ko, Phys. Rev. Lett. **99**, 087402 (2007), erratum: ibid. **103** (17): 179901, 2009.

[13] C. Faugeras, M. Amado, P. Kossacki, M. Orlita, M. Sprinkle, C. Berger, W. A. de Heer, and M. Potemski, Phys. Rev. Lett. **103**, 186803 (2009).

[14] J. Yan, S. Goler, T. D. Rhone, M. Han, R. He, P. Kim, V. Pellegrini, and A. Pinczuk, Phys. Rev. Lett. **105**, 227401 (2010).

[15] C. Faugeras, M. Amado, P. Kossacki, M. Orlita, M. Kühne, A. A. L. Nicolet, Y. I. Latyshev, and M. Potemski, Phys. Rev. Lett. **107**, 036807 (2011).

[16] H. Farhat, S. Berciaud, M. Kalbac, R. Saito, T. F. Heinz, M. S. Dresselhaus, and J. Kong, Phys. Rev. Lett. **107**, 157401 (2011).

[17] A. F. Garcia-Flores, H. Terashita, E. Granado, and Y. Kopelevich, Phys. Rev. B **79**, 113105 (2009), erratum: ibid. **81** (24): 249903, 2010.

[18] P. Kossacki, C. Faugeras, M. Kühne, M. Orlita, A. A. L. Nicolet, J. M. Schneider, D. M. Basko, Y. I. Latyshev, and M. Potemski, Phys. Bev. B **84**, 235138 (2011).

[19] Y. Kim, Y. Ma, A. Imambekov, N. G. Kalugin, A. Lombardo, A. C. Ferrari, J. Kono, and D. Smirnov, arXiv:1112.3884 (2011).

[20] G. Li, A. Luican, and E. Y. Andrei, Phys. Rev. Lett. **102**, 176804 (2009).

[21] P. Neugebauer, M. Orlita, C. Faugeras, A.-L. Barra, and M. Potemski, Phys. Rev. Lett. **103**, 136403 (2009).

[22] D. M. Basko, Phys. Rev. B **78**, 125418 (2008).

[23] D. M. Basko, New J. Phys. **11**, 095011 (2009).

[24] O. Kashuba and V. I. Fal'ko, Phys. Rev. B **80**, 241404 (2009).

[25] M. Mucha-Kruczynski, O. Kashuba, and V. I. Fal'ko, Phys. Rev. B **82**, 045405 (2010).

[26] D. C. Elias, R. V. Gorbachev, A. S. Mayorov, S. V. Morozov, A. A. Zhukov, P. Blake, L. A. Ponomarenko, I. V. Grigorieva, K. S. Novoselov, F. Guinea, and A. K. Geim, Nat. Phys. **7**, 701 (2011).

[27] J. Gonzalez, F. Guinea, and M. A. H. Vozmediano, Mod. Phys. Lett. B **7**, 1593 (1994).

[28] J. Gonzalez, F. Guinea, and M. A. H. Vozmediano, Phys. Rev. B **59**, R2474 (1999).

[29] R. de Gail, M. O. Goerbig, F. Guinea, G. Montambaux, and A. H. Castro Neto, Phys. Rev. B **84**, 045436 (2011).

[30] We thank V.I. Fal'ko for pointing out this possibility.

[31] P. Plochocka, C. Faugeras, M. Orlita, M. L. Sadowski, G. Martinez, M. Potemski, M. O. Goerbig, J.-N. Fuchs, C. Berger, and W. A. de Heer, Phys. Rev. Lett. **100**, 087401 (2008).

[32] A. Grüneis, C. Attaccalite, L. Wirtz, H. Shiozawa, R. Saito, T. Pichler, and A. Rubio, Phys. Rev. B **78**, 205425 (2008).

[33] I. Lobato and B. Partoens, Phys. Rev. B **83**, 165429 (2011).

[34] E. J. Mele, Phys. Rev. B **84**, 235439 (2011).

[35] J. M. B. Lopes dos Santos, N. M. R. Peres, and A. H. Castro Neto, Phys. Rev. Lett. **99**, 256802 (2007).